



Full Length Article

Effects of hydrogen on PAH and soot formation in laminar diffusion flames of RP-3 jet kerosene and its surrogate

Shirong Xin^a, Yong He^{a,b,*}, Wubing Weng^a, Yanqun Zhu^{a,b}, Zhihua Wang^{a,b}

^a State Key Laboratory of Clean Energy Utilization, Zhejiang University, Hangzhou 310027, China

^b Qingshanhu Energy Research Center, Zhejiang University, 311300, Hangzhou, China



ARTICLE INFO

Keywords:

Hydrogen
soot/PAH formation
Aviation kerosene surrogate
PLII/PLIF
Chemical kinetic modeling

ABSTRACT

PAH and soot are harmful substances that can be produced in any type of combustion equipment including aircraft engines. The co-combustion of hydrogen and jet fuel has been applied in aero-engine combustors and large-scale hydrogen addition is a promising solution for reducing the consumption of fossil fuels in the aviation industry. However, it remains unclear how H₂ influences the soot and PAH formation characteristics of jet kerosene. In this study, to investigate the impact of H₂ on soot and PAH formation, planar laser-induced incandescence (PLII), planar laser-induced fluorescence of PAH (PAH-PLIF) and chemical kinetic simulation were conducted for the laminar diffusion flames of RP-3 jet kerosene and its surrogate S1 with different H₂ doping rates. It is found that the introduction of H₂ leads to the increased soot formation. However, the promotion effect of H₂ on the PAH formation weakens as the number of PAH rings increases, and the formation of A4 is significantly inhibited. But the rapidly increase of benzene and alkynes in the H₂-doped kerosene flame may ultimately lead to the promotion of soot formation. Furthermore, the changes in direct synthesis reactions and PAH \Rightarrow PAH- jointly affect the converse changes in A1 and A4 formation. These findings will contribute to the development of the soot model and soot/PAH-reduction strategy for the co-combustion of jet fuels and hydrogen.

1. Introduction

Hydrogen is considered a clean energy as its complete combustion product is only water, and it also has a high flame speed. In the recent decades, hydrogen has been used for co-combustion with aviation fuels to reduce pollutant emissions such as CO and NO_x, while also improving re-ignition performance at high altitudes [1,2]. At the same time, the large-scale co-combustion of hydrogen with aviation fuels is a forward-looking strategy within the aviation industry, which lowers the reliance on fossil fuels and reduces CO₂ emissions. This mitigates the global temperature increase caused by the greenhouse effect [1]. Moreover, considering the expeditious progression of the hydrogen storage industry, the application of large-scale liquid hydrogen in aircraft is also achievable in the near future [3,4].

Polycyclic aromatic hydrocarbons (PAH) and soot are widely recognized as harmful to combustion efficiency, the environment and human health. They can be generated during the incomplete combustion of hydrocarbons in any combustion equipment, including aircraft engines [5–8]. However, the effect of hydrogen on soot formation is closely related to the physicochemical properties of the fuel itself, and it does

not always have an inhibiting effect [9]. For a specific gas additive, the influence on the soot formation in diffusion flame can be generally classified as physical or chemical. The physical effect is mainly demonstrated by the increase of gas volume to lead to a decrease in soot concentration, known as the dilute effect [9,10]. The chemical effect of hydrogen is more complex since it shows different effects on the soot formation depending on the fuel used. Additionally, PAHs are known as the essential precursors in soot nucleation, with the formation process also influenced by the chemical effect of hydrogen. However, the available literature generally focuses on the effect of hydrogen on flame stability and emission reduction [2,11,12], while the mechanisms of soot and PAH generation have rarely been further analyzed. Given that it is unclear how H₂ affects the characteristics of soot and PAH formation in jet kerosene, fundamental studies based on the hydrogen-doped kerosene flame are of great significance.

Co-flow diffusion flames are commonly used to study the soot and PAH formation characteristics of hydrocarbons, which is convenient for chemical kinetic simulation. There are many valuable studies on the chemical effect of hydrogen. Liu et al. [13] performed a numerical study on several axisymmetric co-flow laminar hydrogen-doped methane

* Corresponding author.

E-mail address: Heyong@zju.edu.cn (Y. He).

<https://doi.org/10.1016/j.fuel.2023.130220>

Received 6 June 2023; Received in revised form 24 October 2023; Accepted 27 October 2023

Available online 1 November 2023

0016-2361/© 2023 Elsevier Ltd. All rights reserved.

diffusion flames, and found the H₂ promoted the soot formation compared with helium. The doped hydrogen led to the rapid increase of benzene (A1), pyrene (A4) and acetylene (C₂H₂) and thus enhanced the soot generation in the CH₄ sooting flame. Sun et al. [9] also reported a similar increase in soot volume fraction in several laminar ethylene diffusion flames blended with H₂ using planar laser-based techniques. H₂, compared to N₂, promoted the soot formation. Khanehzar et al. [14] subsequently conducted a numerical simulation for these hydrogen-doped ethylene diffusion flames, and found that the H₂ tended to increase the rate of hydrogen abstraction C₂H₂ addition (HACA) surface growth and PAH condensation under the chemical effects, and thus enhanced the soot formation compared with N₂. However, some studies report converse conclusions. The results of line-of-sight average soot volume fractions measured by Gülder et al. [15] suggested that H₂ didn't show any influence on soot formation in the propane and butane diffusion flames except for its physical effect. In addition, Akram et al. [16] numerically investigated the combustion and emission characteristics of n-dodecane with hydrogen addition. They found that the H₂ mitigated the production of alkynes and suppressed the formation of benzene and pyrene, resulting in a reduction of soot production. Xu et al. [17] performed experimental and numerical studies on hydrogen-doped counter-flow ethylene flames, and found that H₂ has an inhibiting effect on soot formation in ethylene, but the results of certain gas-phase PAH reactions were slightly opposite. Since the chemical effect of hydrogen on soot/PAH formation shows variability in different hydrocarbon flames, the soot/PAH emission characteristics in the H₂-doped kerosene flame are hard to be predicted without experiments.

As the most widely used aviation fuel, aviation kerosene contains hundreds of complex components and the physicochemical properties also show differences because of the different origins and production processes. It is unrealistic to directly simulate the soot/PAH emission characteristics of aviation kerosene. Formulating a surrogate fuel composed of several simple hydrocarbons in specific proportions, highly similar to the aviation kerosene in some combustion characteristics, makes numerical simulations feasible [18–21]. By matching the soot formation characteristics of the surrogate and jet kerosene, further chemical kinetic simulation of the kerosene surrogate can be proceeded to explain the change of reaction pathways of some key radicals in a H₂-doped kerosene flame.

In this paper, PLII, PAH-PLIF were conducted in the co-flow diffusion flames of RP-3 jet kerosene and its surrogate with different hydrogen

doping rates to study the effects of hydrogen on soot/PAH formation of jet fuels. A surrogate was formulated in this work based on the properties of RP-3 kerosene, and the chemical effects of hydrogen were investigated in detail through chemical kinetic simulation, hoping to advance the soot model for the co-combustion of jet fuels and hydrogen and provide some strategies to control the soot and PAH emissions in hydrogen-doped kerosene combustion.

2. Methodology

2.1. Burner and flames

The self-designed gas preheat burner is shown in Fig. 1 and the device components are illustrated in our previous publication [22,23]. The burner can provide hot air co-flow at a high temperature to prevent liquefaction of kerosene or its surrogate inside the jet tube, and this high temperature remains sustained and even throughout the flame. The co-flow temperature is controlled by two electrical heaters and maintained at 600 K. The co-flow air flowrate is kept at 50 L/min. As for the fuel supply, a precise injection pump is used to control the flowrate of liquid fuel, with an accuracy of 0.157 g/h. The liquid fuel flowrate is kept at 4.56 g/h for both RP-3 and the surrogate (S1), and the carbon atom input flow (m_c) of all diffusion flames is kept consistent at 1.084 mg/s. A heater is set at 300 °C to evaporate the liquid fuel, and nitrogen was used as the carrier gas to carry the liquid fuel into the inlet of pre-evaporator, and its flow rate is set as fixed 100 mL/min. The other part of the carrier gas is helium, and its flow rate is adjusted as needed with the introduction of hydrogen. The H₂ doping ratio is realized by changing the volumetric flow rate of hydrogen, defined as $\alpha = \frac{V_{H_2}}{V_{H_2} + V_{carrier}} \times 100\%$. The volumetric flow rate of total gas is kept at 200 mL/min for all studied flames so that the effects of hydrogen on soot/PAH formation are essentially chemical effects. The experiment conditions are shown in Table 1. The H₂ doping ratios calculated based on the fuel heat value are also included, denoted by α_H .

2.2. Optical diagnostics

2.2.1. Planar laser-induced incandescence (PLII)

Fig. 1 shows the setup of the soot-PLII system described in our previous publication [23]. One minor difference is that, a 532 nm laser from

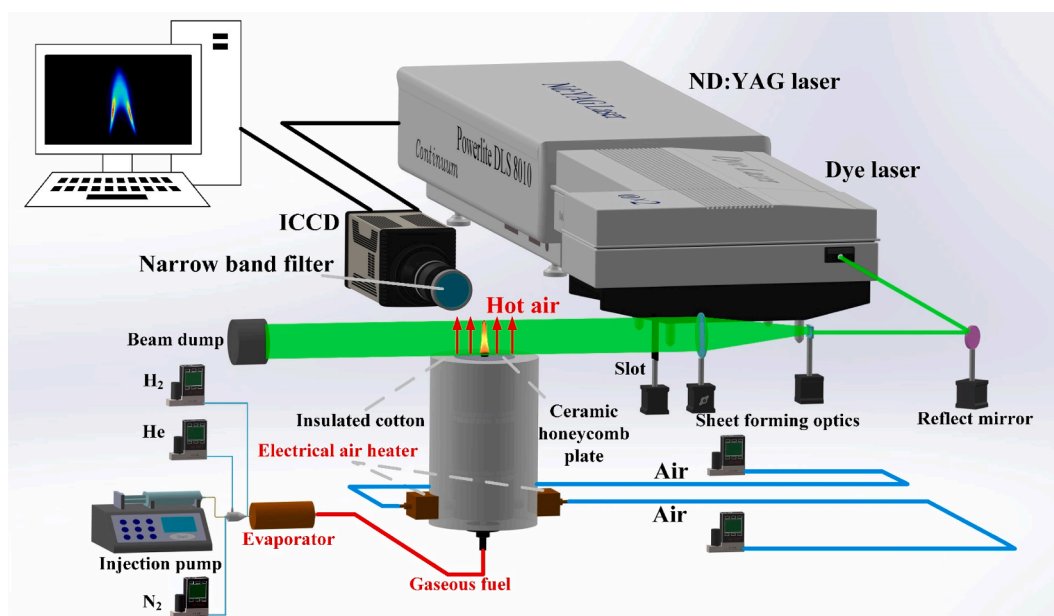


Fig. 1. PLII/PLIF measurement system and gas preheat burner setup for jet fuel.

Table 1
Experimental conditions of jet fuel blended with hydrogen (1 atm, 600 K).

Cases	H ₂ (mL/ min)	Carrier gas (mL/ min)	RP- 3/S1 (g/h)	α (%)	α _H (%)	Co- flow (L/ min)	Preheat temperature (K)
H ₂ -0	0	200	4.56	0	0	50	600
H ₂ - 15 %	30	170	4.56	15	9.13	50	600
H ₂ - 40 %	80	120	4.56	40	21.1	50	600

a 10 Hz Nd:YAG laser (Powerlite DLS 8010, Continuum) is used as the excitation laser. The laser energy density was kept at 0.14 J/cm² to ensure that the LII signal excited was in the saturation regime, and to avoid high-temperature soot sublimation resulting in incandescent intensity decay. Then a concave lens ($f = -30$ mm) and a convex lens ($f = +500$ mm) were used to form a laser sheet with a height of 5 cm and a waist thickness of 200 μm. The soot LII signal was captured by the ICCD camera (PI-max4 emICCD, Princeton Instrument) equipped with a Nikon ultraviolet lens (PF10545MF-UV) and a narrow-band filter (Edmund, central wavelength = 400 nm, FWHM = 25 nm). The ICCD gate width was kept at 100 ns. The time interval between the laser beam and the ICCD camera gate was maintained at 100 ns, to prevent soot LII signals from the interference of PAH laser-induced fluorescence due to the excitation laser at visible wavelength [24]. The 400 nm band filter also helped to reduce the fluorescence interference from other flame species when performing PLII measurement [25]. A beam extinction measurement was performed to acquire a calibration coefficient for converting LII intensity to f_v , and the setup details are the same as our previous work [22].

2.2.2. Planar laser-induced fluorescence of PAHs (PAHs-PLIF)

PAHs-PLIF was conducted for the qualitative measurement of PAH fluorescence. The setup of PAHs-PLIF was similar to the PLII system. A 10 Hz Nd:YAG laser (Powerlite DLS 8010, Continuum) was used to excite Rhodamine 590 dye to produce 283 nm laser after second harmonic. The 283 nm laser was tuned to avoid the excitation of hydroxyl radicals. And the laser pulse energy for PLIF was kept at 2.5 mJ to prevent obvious LII excitation. PAHs fluorescence signals were collected by the ICCD camera with a gate width of 50 ns. Although the 283 nm laser failed to excite the fluorescence of one-ring aromatic hydrocarbons, other kinds of PAHs were unaffected [26]. According to the previous researches [27,28], a 327–353 nm bandpass filter (Edmund, central wavelength = 340 nm, FWHM = 26 nm) was used before the ICCD camera to collect the fluorescence of A2 (naphthalene), a 373–400 nm bandpass filter (Edmund, central wavelength = 386 nm, FWHM = 27 nm) was used to collect the LIF of A3 (phenanthrene), and a 513–538 nm bandpass filter (Edmund, central wavelength = 525 nm, FWHM = 25 nm) was used to collect the LIF of Dimer-A (Dimer-Pyrene or Dimer-Benzo[a]pyrene, the reflection for the efficiency of soot nucleation). 200 collected images were required for each working condition, and the raw PLIF images were corrected according to background noise and the spatial energy distribution of the laser sheet.

2.2.3. Two-color thermometry measurement

Two-color thermometry measurement was used for the measurement of soot temperature and the detail is described in our previous paper [23]. Two ultra-narrow band filters (Andover, central wavelength = 532 nm & 647 nm, FWHM = 1 nm) were used for the ICCD camera to collect the soot luminosity with a gate width of 5 ns. The planar distribution reconstruction of the soot luminosity image mainly relied on the Abel transform [29]. Then the reconstructed luminosity signals were applied to determine the soot temperatures. During calibration, a B-type

thermocouple (Pt/30 % Rh-Pt/10 % Rh) was positioned above a Bunsen flame of methane at the burner center. And the temperature and luminosity signals of thermocouple junction was recorded to determine the calibration coefficient.

2.3. Chemical kinetic modeling

Chemical kinetic simulations were performed based on the Diffusion Opposed-flow Flame Model in CHEMKIN-PRO software [30]. This 1-D model has been commonly used in several publications to simulate the detailed chemical kinetic reactions of diffusion flame [31–34]. For the above reason, Diffusion Opposed-flow Flame Model was adopted in this work to analyze the PAHs formation characteristics of kerosene surrogate fuels. The mechanism developed by Ranzi group [35] was applied for the simulation of gas phase reaction. This mechanism contains 249 species and 8153 reactions, which are up to C20 species. The mechanism is verified in a methane soot flame of [36] and the relevant data is included in the Supplemental Information. In the CHEMKIN-PRO simulation setup, the fuel mass flowrate, temperature, and fuel compositions were consistent with the experimental setup of S1, but the air mass flowrate was kept at one third of the actual co-flow flowrate to ensure the combustion process at a low strain rate. The distance between the outlets of fuel and oxidizer is set to 3.6 cm.

3. Surrogate formulation and evaluation

3.1. Surrogate fuel formulation

RP-3 jet kerosene mainly consists of alkanes and aromatics (typically ~ 30 %). The results of gas chromatography - mass spectrometry (GC-MS) for the RP-3 jet kerosene used in this study are shown in Supplemental Information. The carbon number distribution ranges from C7 to C27, with the alkane distribution varying from C8 to C20. Although the molecular weight is up to 194.85, other physicochemical properties like lower heat value or cetane number meet the national standards of RP-3 aviation kerosene [37]. The formula for RP-3 kerosene is calculated to be C_{13.9}H_{28.08}.

In this paper, n-hexadecane, iso-cetane, and o-xylene are chosen as the surrogate components based on the physicochemical properties and hydrocarbon groups composition of several individual fuels. In order to match the properties of surrogate fuel and jet kerosene such as the gas-phase diffusion characteristics, heat release property, fuel reaction enthalpy and soot formation property, the molecular weight (MW), lower heat value (LHV), H/C ratio, threshold sooting index (TSI), cetane number (CN), and density are used as the selection index for the formulation of surrogate fuel. The soot index is a critical parameter used to assess the sooting tendency of a fuel. Many studies [19–21,33] have demonstrated that using the soot index as one of the selection index for surrogate formulations can successfully replicate the soot-forming characteristics of the jet fuel. So the threshold sooting index is used in the selection index in this work. The calculation equations [21] of these six selection indexes and the objective function of the optimization problem are as follows.

Calculation equations of different selection indexes:

$$MW_{mix} = \sum_i x_i MW_i \quad (1)$$

$$LHV_{mix} = \sum_i w_i LHV_i \quad (2)$$

$$H/C_{mix} = \frac{\sum_i x_i N_{H_i}}{\sum_i x_i N_{C_i}} \quad (3)$$

$$TSI_{mix} = \sum_i x_i TSI_i \quad (4)$$

$$CN_{mix} = \sum_i v_i CN_i \quad (5)$$

$$\rho(T)_{mix} = \sum_i v_i \rho(T)_i \quad (6)$$

Objective function:

$$F = \sum_{j=1}^6 \left[C_j \left(\frac{P_{RP-3} - P_{mix}}{P_{RP-3}} \right) \right]^2 \quad (7)$$

In equations (1) - (7), x_i is the molar fraction of component i , w_i is the mass fraction of component i , v_i is the volume fraction of component i , N_{H_i} is the number of hydrogen atoms of component i , N_{C_i} is the number of carbon atoms of component i , P_{RP-3} is the selection index of RP-3, P_{mix} is the corresponding selection index of components, C_j is the weight of each selection indexes which is set as 1/6. When F is at a minimum value during the iteration, the concentration of each components is output. Finally, the calculated surrogate fuel S1 composes of 30.3 % n-hexadecane, 39.8 % iso-cetane, 29.8 % o-xylene (in mole fraction). The physical properties of the RP-3, surrogate components, and surrogate fuels are shown in Table 2.

3.2. Experimental evaluation

Actual images, soot luminosity images and 2D images of soot volume fraction are shown in Fig. 2, Fig. 3, and Fig. 4, respectively, for all RP-3 and S1 laminar co-flow diffusion flames at different hydrogen doping rates. As shown in Fig. 2, the S1 flame heights are consistent with the RP-3 kerosene flame heights. With increasing hydrogen content in the carrier gas, the flame appearances exhibit similar changes. Unexpectedly, when the blended hydrogen is increased to 40 %, smoke occurs in both RP-3 and S1 diffusion flames, indicating a significant amount of soot generation at this time. The flame brightness in the soot luminosity images (Fig. 3) also shows good similarity, suggesting the relatively minor variations in the thermal radiation of the flames. A disadvantage of luminosity imaging arises from the disappearance of soot luminosity in the upper regions of the H₂-40 % flames due to their lower temperature. The 2D distributions of soot volume fraction (f_v) (Fig. 4) show that S1 also exhibits a good reproducibility in terms of the f_v distribution characteristics of the RP-3 kerosene. The higher soot concentrations are always found at the two sides of the flames (flame wings) [9], corresponding to the soot luminosity in this flame front where the soot thermal brightness is always strongest, while the soot distribution is relatively uniform within the flames. Importantly, the variations in f_v with increasing blended hydrogen are highly similar in both RP-3 and S1 flames, suggesting the significance of the chemical kinetic mechanism of S1 for further investigation of the PAH/soot formation characteristics of jet kerosene.

Table 2

Selection indexes value of the RP-3, surrogate components, and surrogate fuels.

Selection indexes value	RP-3	n-hexadecane	iso-cetane	o-xylene	S1
MW (g/mol)	194.85	226.44	226.44	106.17	190.55
LHV (MJ/kg)	42.34	43.95	43.85	40.8	43.38
H/C	2.02	2.13	2.13	1.25	1.97
TSI	25.87	8.58	22	47	25.38
CN	45	100	15	8.3	44.81
viscosity (mm ² /s, 20 °C)	2.38	4.27	4.69	0.92	2.8
density (g/cm ³ , 20 °C)	0.79	0.79	0.78	0.86	0.8

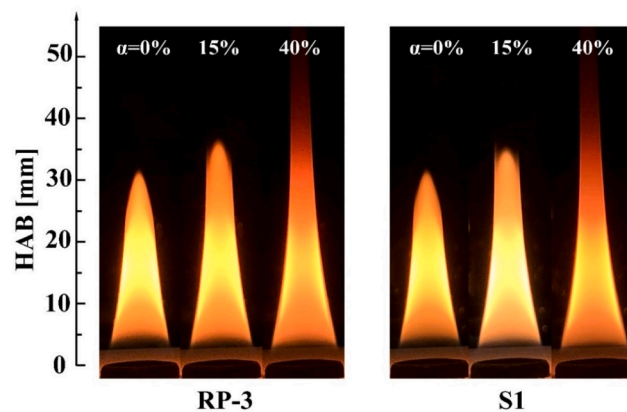


Fig. 2. Laminar co-flow diffusion flames of RP-3 jet kerosene and its surrogate at different hydrogen doping rates.

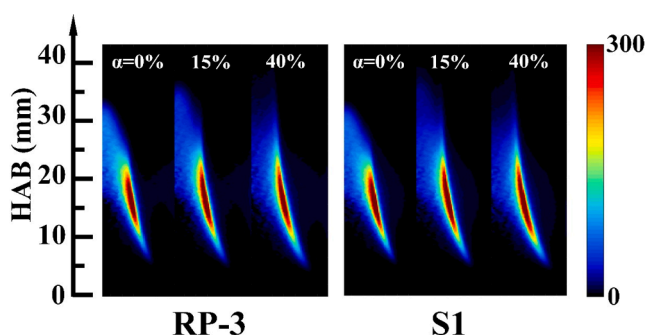


Fig. 3. Soot luminosity images recorded at the wavelength of 647 nm.

4. Results and discussion

4.1. Soot volume fraction (f_v) and soot temperature

Fig. 5 shows the soot volume fraction (f_v) along the burner centerline with different hydrogen doping rates. The f_v in the axial direction of all studied flames initially increases and then decreases with increasing height above the burner (HAB). With increasing hydrogen content in the fuel, the soot concentration gradually increases along the centerline. Besides, the slightly lower initial axial position where soot starts to generate suggests the earlier start time for soot inception at higher hydrogen content. The greater residence height also means longer residence time interval for soot maturation. Correspondingly, the higher flame height may suggest the promoting effects of hydrogen on the expansion of the regions for soot growth.

Fig. 6 presents the radial profiles of soot volume fraction (f_v) with different hydrogen doping rates at different flame heights. As seen in the radial profiles, the maximum f_v always presents at the flame wing sides. At HAB = 12 mm, the radial LII signal is strong enough, suggesting that there is already soot formation near the burner exit. As HAB increases, the f_v peak becomes flat, meaning the gradual decay of the wing side. With increasing H₂, at any height, the radial f_v peaks increase sharply, revealing that the promoting effects of hydrogen on soot concentration are relatively significant. For a given additive, its effects on soot formation can be categorized into dilution, thermal and chemical effects [38,39]. For the inert gases like nitrogen and argon, only physical effects are present in the flame, mainly dilution and thermal effects, since the inert gases don't participate in any chemical reactions during soot inception [40]. But for the active additives, these three effects exist simultaneously in the process of soot/PAH generation. In this work, the volumetric flow rate of total gas remains constant to maintain the same physical effects in all studied flames. Consequently, in this current work,

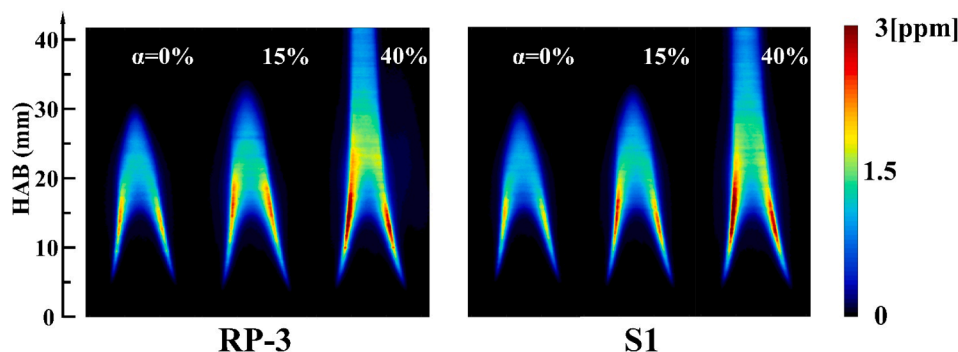


Fig. 4. Two dimensional distributions of soot volume fraction with increasing hydrogen.

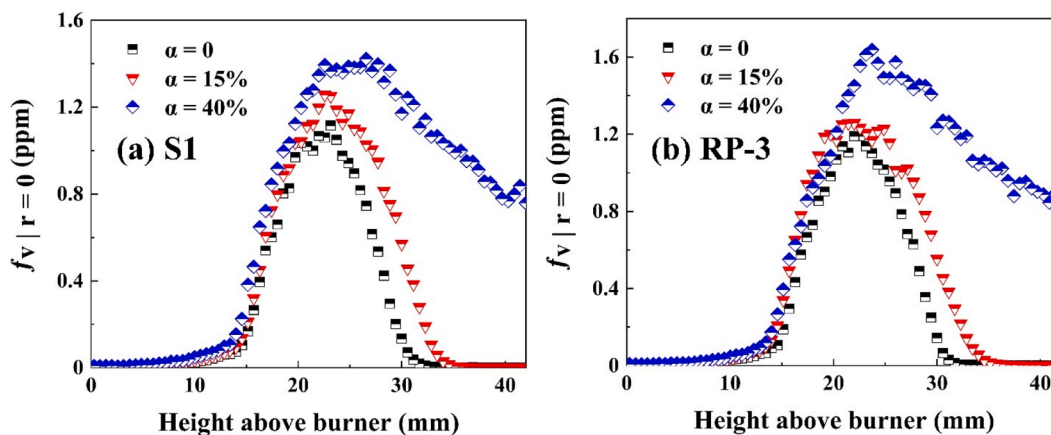


Fig. 5. Soot volume fraction (f_v) along the burner centerline with different hydrogen doping rates.

the promotion effects of hydrogen on soot formation are mainly chemical effects, which helps for subsequent chemical kinetic analysis in the following sections.

Fig. 7 illustrates the radial temperature distribution of soot within the S1 flames at different HAB. The entire soot temperature distribution can be divided into two distinct regions: one being the internally uniform temperature region, and the other being the wing region near the flame front with significantly higher temperatures. With an increase in the hydrogen doping level, a clear trend emerges: the temperature within the flame core decreases, while the temperature near the flame front correspondingly increases. The sudden temperature increase near the flame wing is attributed to the intense exothermic reaction between jet-fuel/hydrogen and air. Importantly, due to substantial differences in the molar concentrations of jet fuel and hydrogen in this study, the impact of increased hydrogen doping on the soot temperature near the flame wing becomes pronounced. Meanwhile, the decrease in temperature in the internal region may be associated with a slight enhancement in soot thermal radiation. As the hydrogen content increases, the concentration of soot in the internal region also rises, resulting in an increase in radiative losses of the internal flame region. However, unlike the flame wing, there is not enough air supply to support exothermic reactions within the internal region, causing a slight decrease in internal flame temperature. The decrease in internal temperature may suggest reduced oxidative consumption of soot in the internal region. As shown in the added OH-PLIF data in Supplemental Information, the decrease of OH-LIF signals in the internal region with increasing hydrogen doping corresponds to the trend of the internal temperature. In contrast, OH-LIF in the wing region rapidly increases with increasing hydrogen doping, corresponding to an increase in flame front temperature. Furthermore, the rapid increase in soot concentration in the wing region may be related to an extended residence time in the high-temperature region.

The figure of average soot temperatures at different heights is included in the submitted Supplemental Information. With increasing hydrogen doping, the length of the high-temperature (>1400 K) region increases, indicating a slightly extended residence time in the high-temperature region, promoting the growth of soot and PAHs.

4.2. Overall soot formation

The carbon conversion factor η was used to evaluate the propensity of fuel to soot, which represents the percentage of carbon converted to soot [41]. The calculation equations of η are as follows:

$$\eta = \frac{m_s}{m_c} \quad (8)$$

$$m_s = v_h \rho_s \int 2\pi f_v(r, h) r dr \quad (9)$$

$$v_h = (v_{fuel}^2 + 2ah)^{\frac{1}{2}} \quad (10)$$

$$t = \frac{v_h - v_{fuel}}{a} \quad (11)$$

where m_c is the total mass flow rate of carbon, kept at 1.084 mg/s for all flames mentioned in Section 2.1. m_s is the mass flow rate of carbon converted to soot, calculated by the axial velocity v_h , the soot particle density ρ_s (set as 1900 kg/m³ [42]), and the row integral of soot volume fraction at a certain height. Soot residence time t is determined by the axial velocity, the initial fuel velocity v_{fuel} , and the buoyancy acceleration a (constant at ~ 25 m/s² [43]).

Fig. 8 presents the profiles of carbon conversion factor η versus residence time with different hydrogen doping rates. It is obvious that as

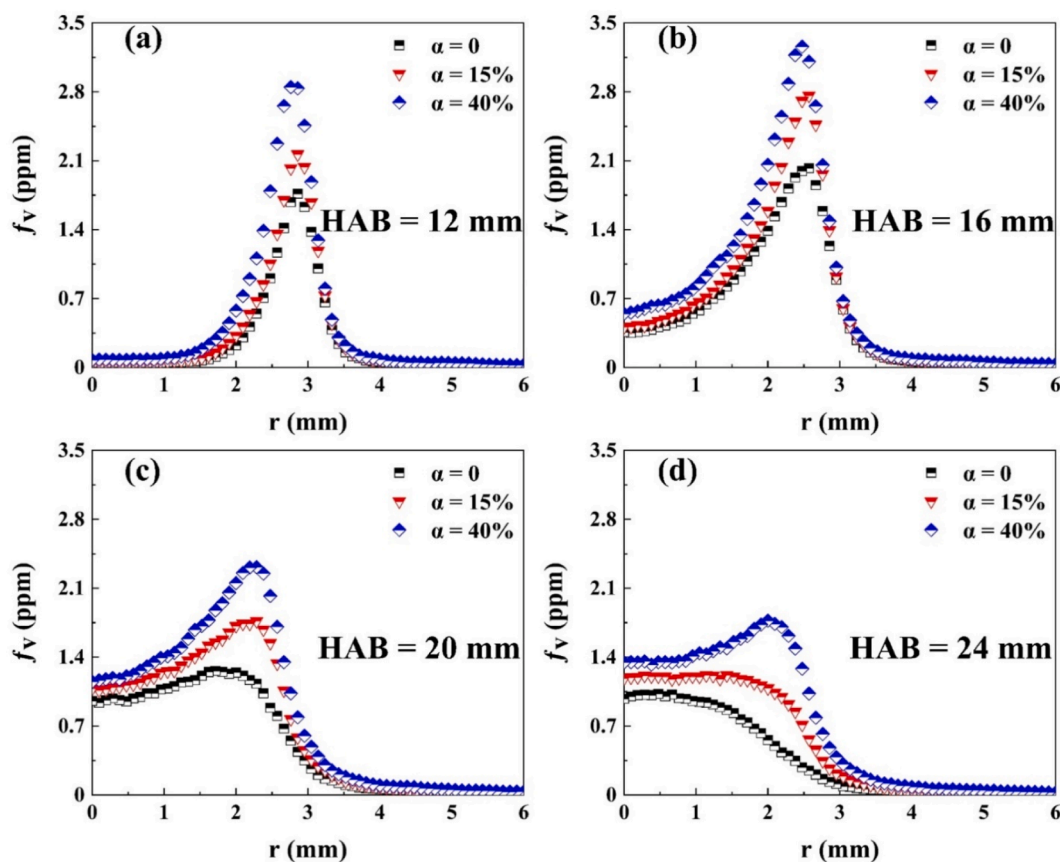


Fig. 6. Radial profiles of soot volume fraction (f_v) at different height above burner (HAB).

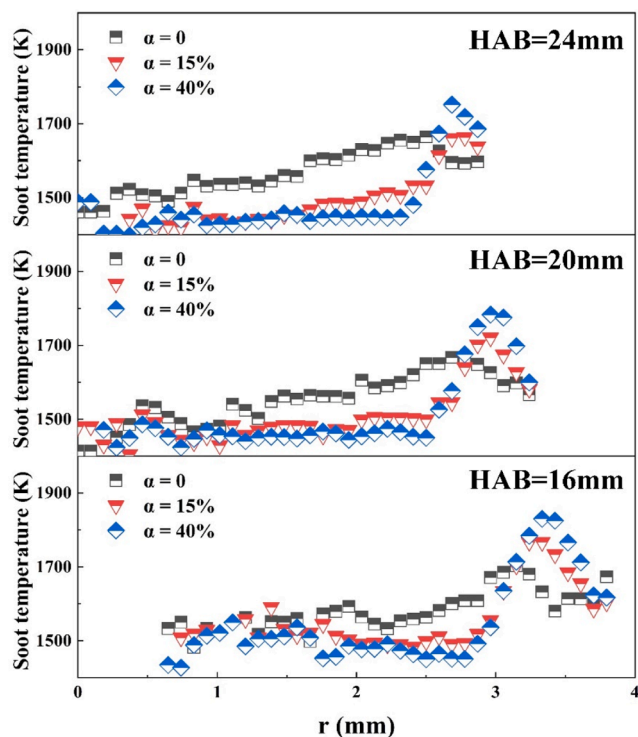


Fig. 7. Radial profiles of soot temperature with different hydrogen doping rates.

H_2 increases in the flames, the carbon conversion factor η increases, suggesting a large percentage of carbon converted to soot. Besides, the residence time interval for η from 0.001 increases to its peak value also increases, providing enough time for soot inception and maturation. This means that the hydrogen significantly enhances the propensity of jet fuels to soot, and this enhancement is closely related to the chemical effects of hydrogen.

In order to clearly explain the effect of H_2 on the soot formation, the soot volume content $f_{v|vol-int}$ (total soot loading) in all studied flames is calculated based on the 2D f_v distribution measured by LII, and the calculation equations is as follows [22]:

$$f_{v|vol-int} = \int_0^{\infty} dh \int_0^{\infty} 2\pi f_v(r, h) r dr \quad (12)$$

As shown in Fig. 9, it can be clearly observed that the total soot loading presents a linear increase with the increase of hydrogen doped in both RP-3 and S1 flames. At $\alpha = 40\%$, the total soot loading in the RP-3 flame increases by 2.19 times that of the pure jet fuel flame, while the S1 flame increases by a factor of 2.25. As for maximum soot concentration, $f_{v,max}$ in the RP3 flame increases by a factor of 1.44 while the S1 flame increases by a factor of 1.56. It is obvious that hydrogen always contributes to the increase of soot generation, both at the flame front and in the overall flame. The similar conclusions can be found in the LII measurement results of Sun et.al. [9] and the simulation work of Liu et.al. [13], despite studying simple ethylene flames and methane flames, respectively. It is important to note that hydrogen has varying chemical effects on soot formation due to the differences in soot precursor formation among various types of fuels. Therefore, the precise chemical function of hydrogen in the precursor formation of jet fuel is crucial.

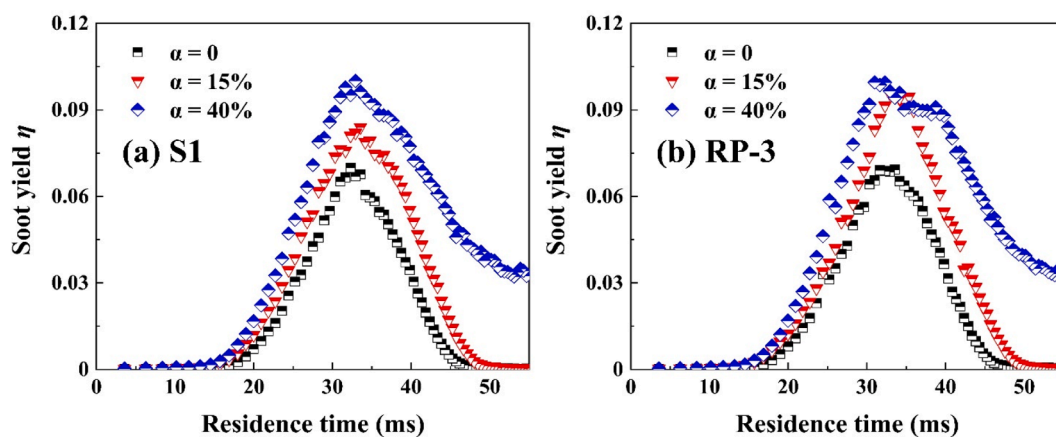


Fig. 8. Percentage of carbon converted to soot, i.e., carbon conversion factor η versus residence time with different hydrogen doping rates.

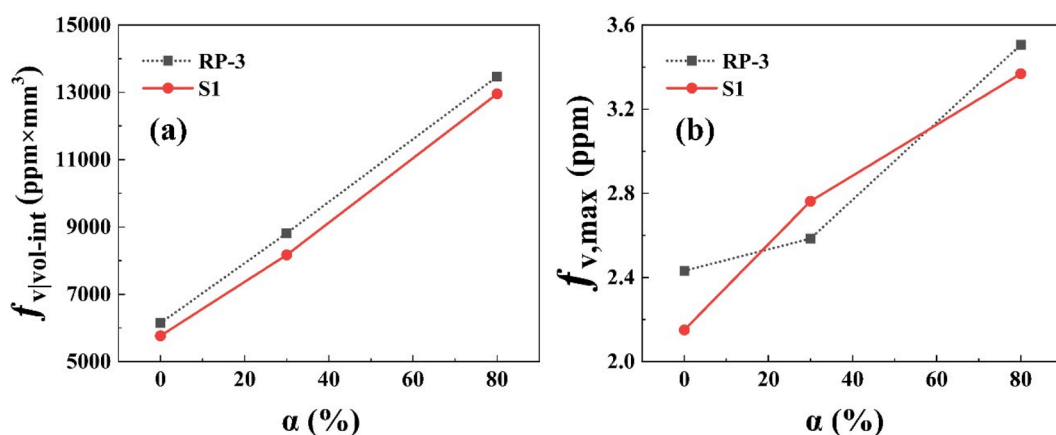


Fig. 9. (a) Total soot loading ($f_{v|vol-int}$) and (b) maximum f_v ($f_{v,max}$) with different hydrogen doping rates.

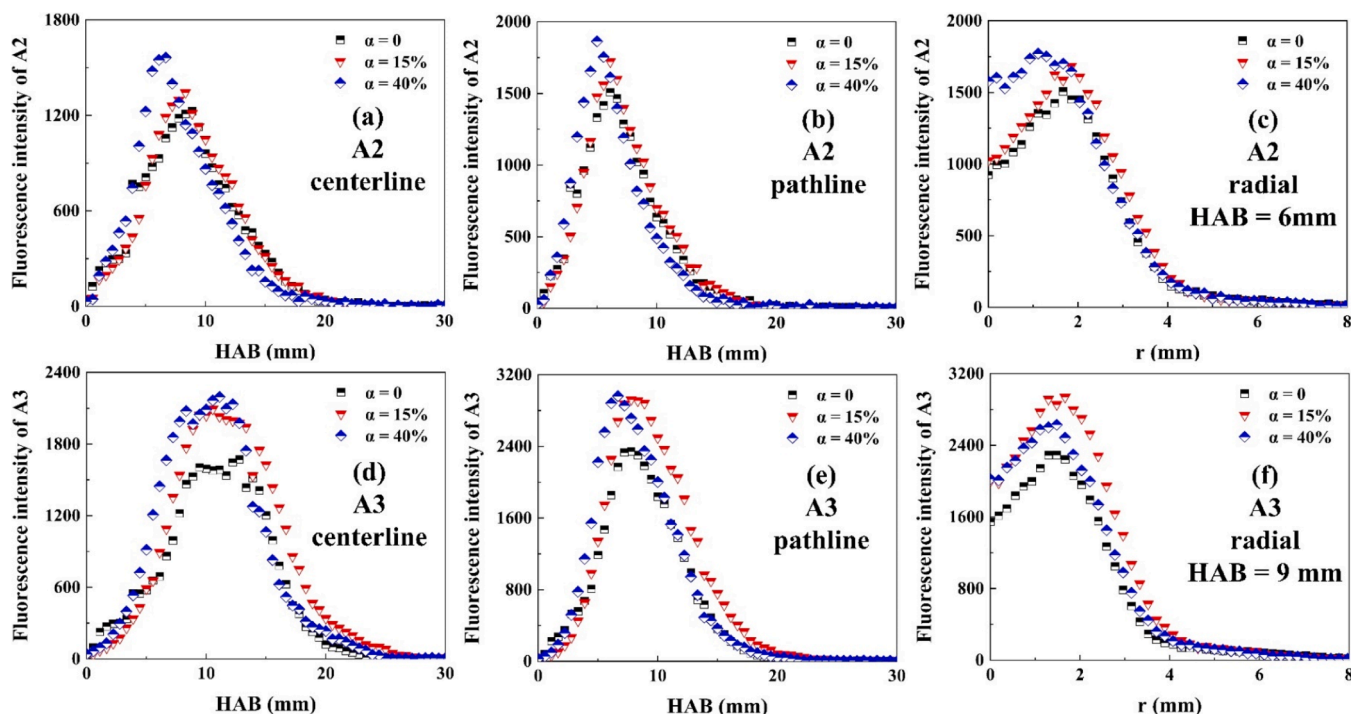


Fig. 10. Fluorescence intensity of A2 and A3 at different axial and radial positions.

4.3. Polycyclic aromatic hydrocarbon (PAH)

Fig. 10 presents the fluorescence intensity of A2 and A3 along different axial and radial positions of S1 flames. As shown in Fig. 10, it is found that the axial LIF signals of both A2 and A3 gradually disappear beyond 15 mm due to soot formation. Importantly, with increasing hydrogen doping rates, the initial axial position of both A2 and A3 formation shifts upstream closer to the burner exit. This means that the blending of hydrogen promotes earlier fuel decomposition and faster PAH generation, resulting in enhanced PAH adsorption for earlier soot formation. This tendency is consistent with the change of the carbon conversion factor. Additionally, the influence of hydrogen on the peak of fluorescence intensity is relatively obvious in the axial and radial profiles of A2, whereas the peak of the A3 fluorescence signals no longer rises at $\alpha = 40\%$. In Fig. 10 (f), at HAB = 9 mm, the A3 peak for the radial profile of the H₂-40% flame even decreases. This suggests that the formation of larger PAH like phenanthrene can't be promoted by the excess hydrogen, and it stagnates instead.

However, the blending of hydrogen always promotes the formation of dimer-PAH, as presented in Fig. 11. Due to the complex spatial and chemical structure, the fluorescence of dimer-PAH primarily spreads across the visible wavelength band, mitigating the interference of other fluorescence. In Fig. 11, the promotion effect of hydrogen is very similar in both kerosene and S1 flames. Besides, when comparing to A2 and A3 referred to Fig. 10, dimer-PAH forms at a higher initial axial position, which is consistent with the fact that the dimer-PAH is produced after the small PAH. Although the pathways of gas-phase hydrocarbon precursors to high-temperature carbonaceous-particle are disputed, the most popular point is that the collision of two gaseous PAH results in the initial soot nucleation through the effects of radicals with extended conjugation [44], and the dimer carbonization by PAH-PAH bond [45] is a critical process. Therefore, the change of dimer-PAH can reflect the efficiency of soot inception. But it is interesting to note that although the excess hydrogen stagnates the increase of larger individual PAHs (A3), the increase of dimer-PAH is not affected, and the soot inception is always promoted. It seems that the soot nucleation in jet fuel flames is not dependent only on the combination of large PAHs like phenanthrene,

and conversely, different kinds of PAHs in jet fuel flames may participate in the process of soot inception. This needs more discussion of various PAHs which will be presented in section 4.4.

A more visual comparison can be seen in the Fig. 12, which shows the maximum intensity of PAHs-LIF and the peaks of radial-integrated intensity along the flame height. Values are normalized based on the value at $\alpha = 0$. As shown in Fig. 12, the peak signals of A2 and dimer-PAH can be kept increasing linearly with the increase of hydrogen doping rate. But different from A2, the stagnation in A3 concentration can be clearly seen at $\alpha = 40\%$, both the maximum intensity and the maximum radial-integrated intensity. Although the maximum intensity of A3 fluorescence increases rapidly when 15% H₂ is blended, it stops increasing after the addition of 40% H₂, unlike the linear increase in A2 or Dimer-PAH.

4.4. Simulation analysis

The S1 flames with different hydrogen doping rates are simulated by CHEMKIN-PRO for analyzing the chemical effect of hydrogen on PAH formation. Fig. 13 shows the simulation results of A1 (benzene), A2 (naphthalene), A3 (phenanthrene) and A4 (pyrene). It is clear that the doped hydrogen results in the upstream shift of A1-A4 generation region closer to the fuel jet exit. This is interestingly similar to the findings of LIF experiments shown in Fig. 10, indicating the promotion effects of H₂ on the earlier soot/PAH formation. Importantly, hydrogen shows different effects on the formation of different PAH. For A1 and A2, the blending of hydrogen leads to the enhancement in the peak mole fraction of A1 and A2, while for A3, 15% H₂ increases the A3 mole fraction but 40% H₂ slightly lowers the A3 mole fraction, indicating a stagnation in A3 formation. This is interestingly similar to the tendency in the fluorescence intensity of A2 and A3. A more interesting example is the change in the mole fraction of A4. Hydrogen suppresses the formation of A4, leading to the significant decrease of A4 mole fraction. This suggests that the enhancing effect of hydrogen on PAH generation is weaker with the increasing ring numbers in PAH molecule, and the inhibiting effect on A4 formation is relatively obvious.

However, considering the enhancing effect of hydrogen on the

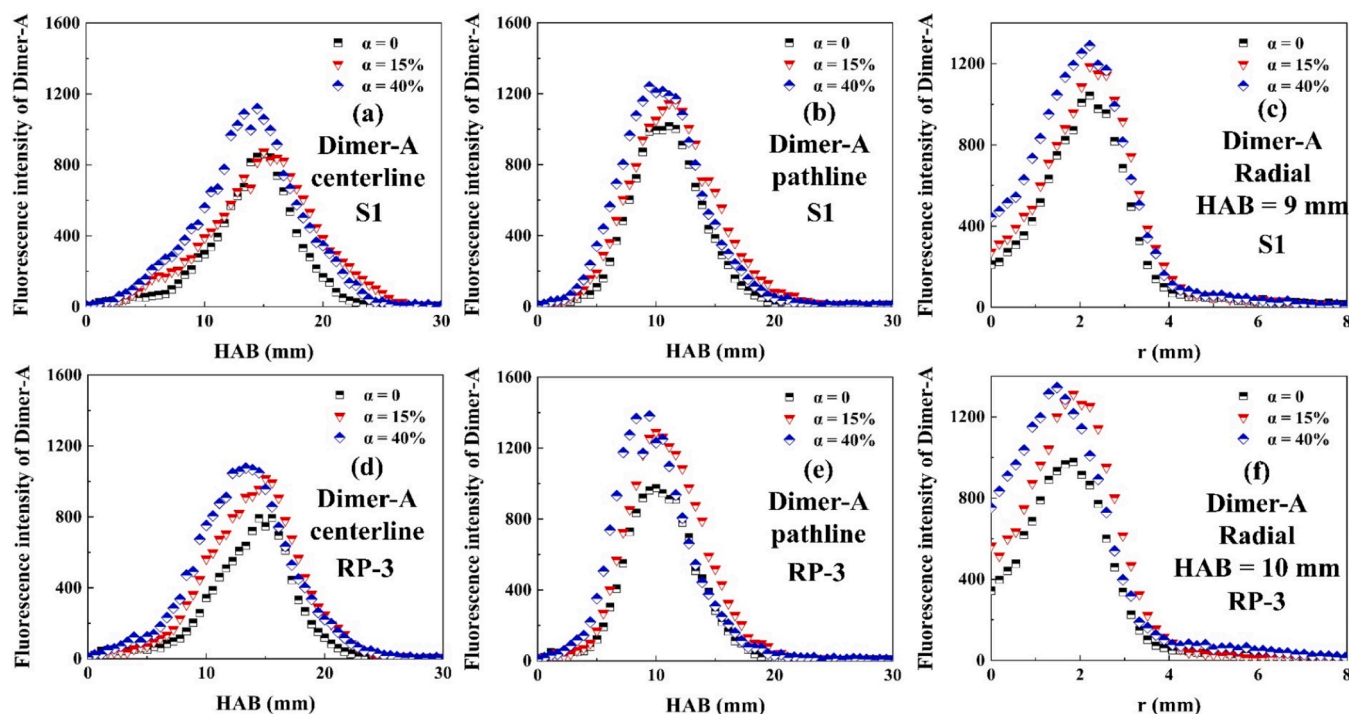


Fig. 11. Fluorescence intensity of Dimer-PAH at different axial and radial positions.

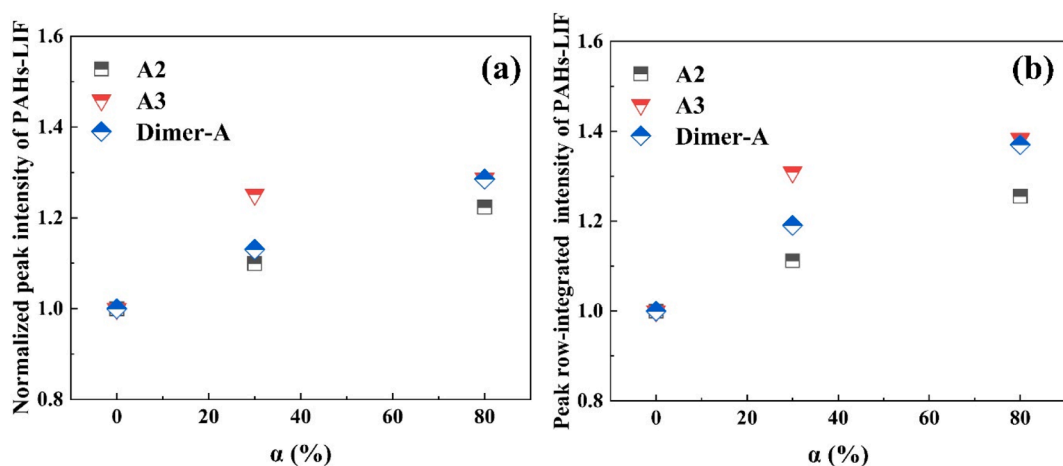


Fig. 12. (a) Normalized maximum intensity of PAHs-LIF, and (b) peaks of the curves for cumulative sum along radial PAHs-LIF line profiles versus HAB, normalized based on the value at $\alpha = 0$.

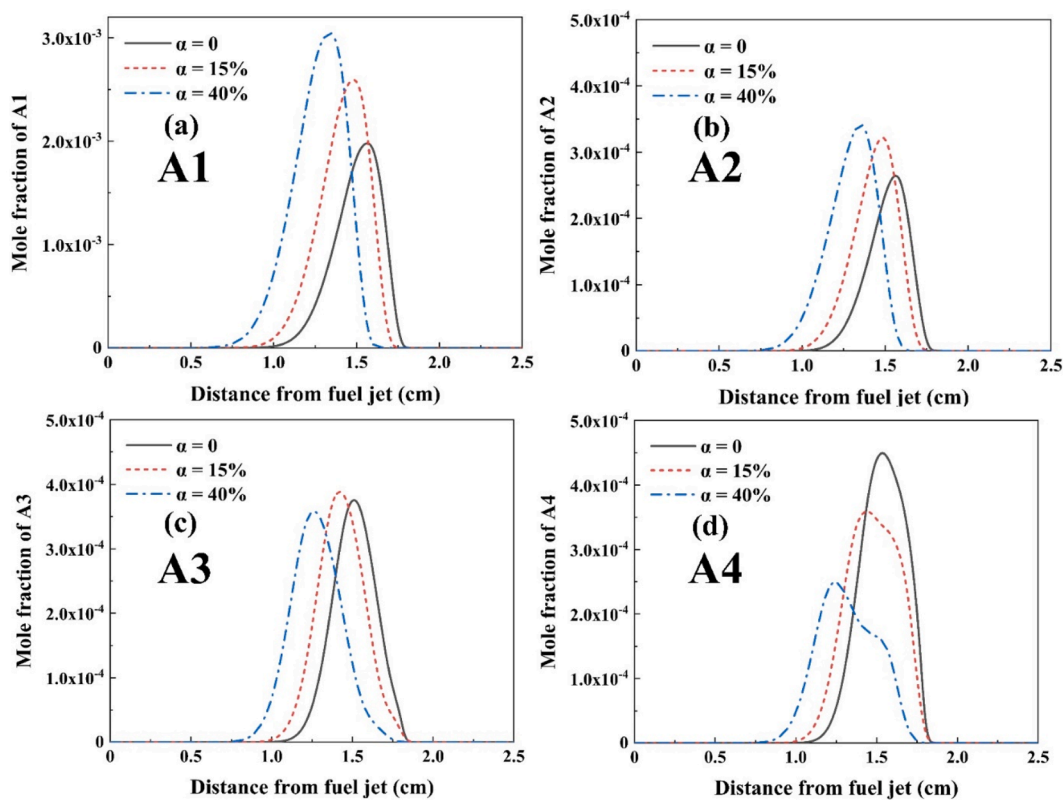


Fig. 13. Simulated mole fraction profiles of PAHs with different hydrogen doping rates.

formation of Dimer-PAH in Fig. 11, it can be found that the soot inception is not diminished although the PAH such as pyrene decreases. In soot flames, all gas-phase PAHs have the potential to participate in the process of soot inception. In other words, soot inception from all PAHs rather than individual PAHs is more reasonable [45]. But as conclusions in the study of Kholghy et al. [45], small PAH such as A1, plays a very important role in the formation of dimers, and contributes substantially to the concentrations of soot nucleation, which is validated experimentally and numerically. In Fig. 13, the hydrogen significantly enhances the mole fraction of A1, and as a result, the promotion effect of rapidly increased A1 on soot inception offsets the negative effect of rapid decrease in other PAHs, probably resulting in a slight increase in the concentrations of soot nucleation. Additionally, the recent studies of

Frenklach et al. [46–48] revealed a new mechanism of soot nucleation, which indicated the reactions between the two PAH moieties enhanced through a doubly-bonded bridge, important than direct A4 dimerization. The E-bridge theory developed by Frenklach group provided a rich theoretical explanation for dimer formation, highly enlightening for the current research. The such process is based on HACA, probably affected by the dissociated H and the formation of monomer PAH with a five-member ring during the bridging step. In the H_2 -doped kerosene flames, the large number of dissociated H and increased ethylene may facilitate the formation of bridged PAH clusters [46] through H Abstraction and the formation of accepyrenyl, which may contribute to the soot nucleation. The change in H and ethylene with increasing doped hydrogen can be seen in the Supplemental Information. However, due to

the lack of enough computational resources and detail PAH mechanism for larger PAH formation in H₂-doped kerosene, more detailed evidence of the nucleation process awaits further modelling studies in the future.

But the nucleation may not be the only contributing factor to the rapid increase of soot. According to the detailed numerical study of Khanehzar et al. [14], surface growth and PAH condensation are responsible for the change in soot volume fraction when hydrogen is introduced. They found that the surface growth rate significantly increases under the chemical effects of hydrogen. Fig. 14 presents the simulated mole fraction of C₂H₂ and total alkynes. It can be seen that hydrogen substantially contributes to the formation of abundant alkynes. These abundant C₂H₂ would significantly promote the process of soot surface growth through the mechanism of hydrogen abstraction C₂H₂ addition (HACA) [13], and in a way, promote the rapid increase of soot.

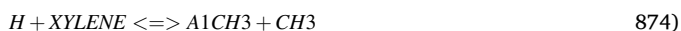
To further explain the difference in chemical effects of H₂ on different PAHs, Fig. 15 and Fig. 16 respectively show the reaction sensitivity coefficients and main reaction pathways responsible for A1-A4 formation at ~ 1400 K. At this temperature, the mole fractions of A1-A4 reach their maximum and the PAHs gradually proceed to soot nucleation. In Fig. 15, the positive sensitivity coefficient represents the positive effect of a reaction on the formation of a certain PAH, and the negative sensitivity coefficient represents the inhibiting effect. As seen in Fig. 15, the reactions most sensitive to promote and suppress the A1 formation are:



This means the reversible reaction $A1 \rightleftharpoons A1-$ is critical for the stability of A1. In addition, as seen in the pathways of A1 in Fig. 16, the main reactions for the synthesis of A1 are:



These reactions suggest two primary pathways for the synthesis of PAH. The C₃H₃ mainly comes from the radical pool formed through the decomposition of alkanes in surrogate S1. These small radicals synthesized the first benzene ring. The other pathway is motivated by A₁CH₃, which mainly comes from the decomposition of o-xylene (29.8 %, in mole fraction) in S1:



But with increasing hydrogen doping rates, R408 is replaced by R874 in the reactions most sensitive to synthesize A1, and correspondingly, R584 gradually becomes an essential reaction for the A1 formation, as seen in the change in positive sensitivity coefficients of A1. This means

with more doped hydrogen, the o-xylene decomposition has an increasing contribution to the synthesis of A1.

As for A2-A4, the reversible reactions $A2 \rightleftharpoons A2-$, $A3 \rightleftharpoons A3-$, $A4 \rightleftharpoons A4-$ are still critical. For example, in Fig. 15 (b), for the H₂-40 % flame, reactions most sensitive to promote and suppress the A2 formation are:



The HC₂A₁- generated through R4581 promotes the A₂- formation by R919: $HC2A1 + C2H2 \Rightarrow A2-$, and thus indirectly promotes the reverse of $A2 \rightleftharpoons A2-$. Hence it can be seen that the $A2 \rightleftharpoons A2-$ is significant for A₂ formation. Similarly, as seen in the pathways of A₃ and A₄ in Fig. 16, the conversion between A₃/A₄ and A₃-/A₄- is also important for A₃/A₄ formation and the main synthesis reactions of A₂-A₄ are closely related to the o-xylene. And for the A₃ and A₄ formation, the rapid increase can be found in the sensitivity coefficients of reactions related to the RXYLENE generation such as $H + XYLENE \Rightarrow H2 + RXYLENE$ and $XYLENE \rightleftharpoons RXYLENE + H$. This means the concentration of RXYLENE becomes increasingly important for the synthesis of A₃ and A₄ with increasing hydrogen doping rates.

From the above analysis, it can be concluded that the PAH formation in S1 flame is jointly governed by the reactions of $PAH \rightleftharpoons PAH-$ and the synthesis reactions stimulated by o-xylene. Therefore, Fig. 17 (a) presents the changes in the mole fraction of A₁CH₃ and RXYLENE and Fig. 17 (b) shows the rate of increase in K, the ratio of the ROP for $PAH + H2 \Rightarrow PAH + H$ to the ROP for $PAH + H \Rightarrow PAH + H2$, i.e.

$$K = \frac{ROP(PAH - + H2 \Rightarrow PAH + H)}{ROP(PAH + H \Rightarrow PAH - + H2)} \quad (13)$$

This value represents the ratio of the rate of production and consumption of a certain PAH with the participation of H₂ and H. It can be used as an evaluation of the stability of a given PAH as the doped hydrogen increases. K value is normalized based on the values at $\alpha = 0$.

As shown in Fig. 17 (a), with increasing H₂ doping rates, the mole fraction of A₁CH₃ increases, while the mole fraction of RXYLENE decreases. This is due to the large amount of H which drives R874: $H + XYLENE \rightleftharpoons A1CH3 + CH3$ in a forward direction but drives R774: $XYLENE \rightleftharpoons RXYLENE + H$ in a reverse direction. This indicates that the hydrogen promotes the decomposition of o-xylene in the formation of one-ring benzene but inhibits the direct synthesis of A₂-A₄ stimulated by o-xylene. Moreover, as presented in Fig. 17 (b), there are large differences in the stability of different PAHs with the introduction of H₂. The K values of A₁ and A₂ increase obviously as the doped hydrogen increases, which means the inhibiting effect of hydrogen on the decomposition of A₁ and A₂. But interestingly, the increase in K value of A₃ shows a stagnation in the H₂-40 % flame, which corresponds to the

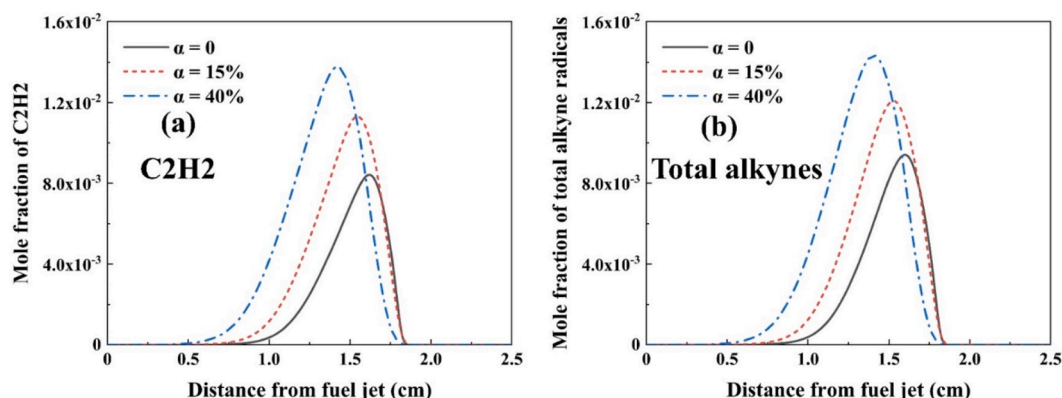


Fig. 14. Simulated mole fraction profiles of (a) C₂H₂ and (b) total alkynes.

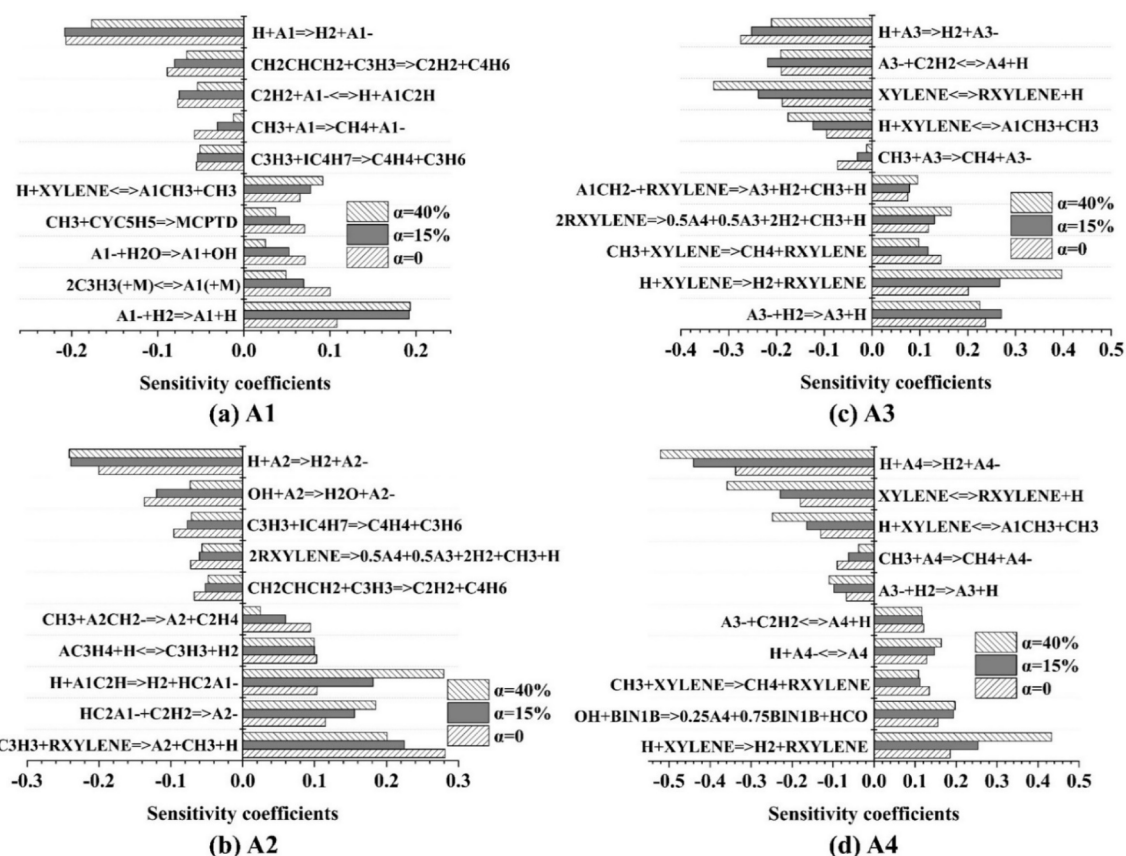


Fig. 15. Sensitivity analysis of A1-A4 formation at ~ 1400 K.

change in A3 mole fraction discussed before. However, for the change in K value of A4, there is a gradual reduction with increasing H_2 doping rates. This suggests the inhibiting effect of hydrogen on the decomposition of PAH becomes increasingly weaker with the increasing ring numbers in PAH molecule. Thus for A4, as the doped hydrogen increases, the decrease of ROP for the direct synthesis of A4 and the unsustainable stability of A4, jointly result in the reduction of A4 mole fraction. Conversely, the rapid increase of A1 mole fraction is closely related to the increase in the decomposition of o-xylene and the increasingly stronger stability of A1 with the doped H_2 .

5. Conclusions

In this study, the soot and PAH formation in laminar diffusion flames of RP-3 jet kerosene and its surrogate S1 with different H_2 doping rates were investigated experimentally and numerically at 600 K and atmospheric pressure. The study aims to contribute to the development of the soot model for the co-combustion of jet fuels and hydrogen. The main outcomes of the effects of H_2 on the formation of soot and PAH in jet fuel are summarized as follows.

- (1). The blending of H_2 in the diffusion flame of jet fuel leads to a higher flame height and an enhancement of both maximum f_v and total soot loading, indicating the promotion effect of hydrogen on soot formation. As H_2 increases, more carbon is converted into soot. Besides, the maximum residence time interval of the flames also increases, providing enough time for soot inception and maturation.
- (2). As the H_2 doping rate increases, the PAH formation zones shift upstream closer to the burner exit, correlating with the change in the carbon conversion factor. Similarly, the simulated PAH formation zones also present such change.

- (3). Different PAHs have different sensitivities to the H_2 blending. With A2 and dimer-PAH LIF increasing linearly with H_2 doping rates, A3 LIF intensity growth shows stagnation clearly in H_2 -40% flame. According to the analysis of 1-D simulation, the promotion effect of hydrogen on the generation of PAHs weakens with the increasing ring numbers in PAH molecule, and the inhibiting effect on the formation of A4 is obvious.
- (4). The rapidly increase in A1 and C2H2 may ultimately promote the increase of soot in the flames. But the competition between different pathways need more detailed soot nucleation modeling in the future to provide more evidence.
- (5). The formation of PAH is jointly governed by the reactions of $PAH \rightleftharpoons PAH^-$ and the synthesis reactions stimulated by o-xylene (29.8% in S1). The hydrogen promotes the decomposition of o-xylene during the A1 formation, but it inhibits the direct synthesis of A2-A4. Moreover, the inhibiting effect of hydrogen on $PAH \rightarrow PAH^-$ weakens increasingly with the increasing ring numbers in the PAH molecule. These finally result in the converse change of A1 and A4 formation.

CRedit authorship contribution statement

Shirong Xin: Writing – original draft, Formal analysis, Data curation. **Yong He:** Conceptualization, Investigation, Methodology, Validation, Writing - review & editing. **Wubing Weng:** Writing – review & editing. **Yanqun Zhu:** Writing – review & editing. **Zhihua Wang:** Funding acquisition, Investigation, Writing - review & editing.

Declaration of Competing Interest

The authors declare that they have no known competing financial interests or personal relationships that could have appeared to influence

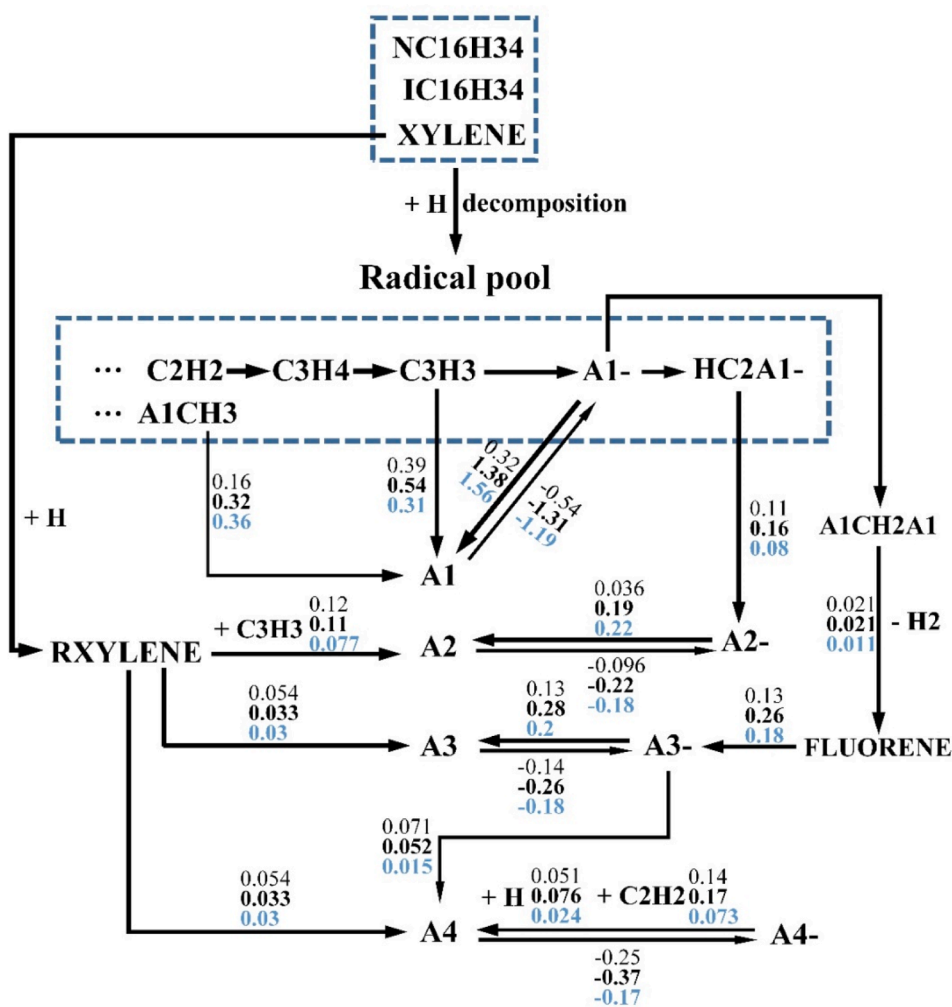


Fig. 16. Main reaction pathways of A1-A4 formation at ~1400 K. The number on the arrow represents the rate of production (ROP) in $10E-7$ mol/cm³-sec (H₂-0, regular font; H₂-15 %, black bold font; H₂-40 %, blue bold font).

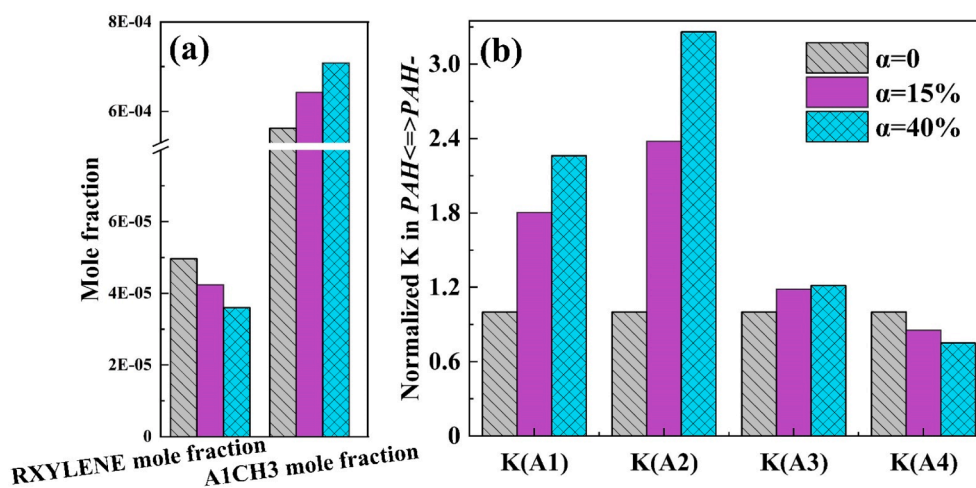


Fig. 17. (a) The changes in mole fraction of RXYLENE and A1CH3 with different H₂ doping rates. (b) K values in $PAH \rightleftharpoons PAH-$, the ratio of the ROP for $PAH + H_2 \rightarrow PAH + H$ to the ROP for $PAH + H \rightarrow PAH + H_2$, normalized based on the values at $\alpha = 0$.

the work reported in this paper.

Data availability

Data will be made available on request.

Acknowledgments

This work was supported by the Zhejiang Provincial Natural Science Foundation of China (LZ21E060003, LR23E060001) and National Natural Science Foundation of China (52125605). Authors also thank the support from the Fundamental Research Funds for the Central Universities (2022ZZFJH004).

Appendix A. Supplementary data

Supplementary data to this article can be found online at <https://doi.org/10.1016/j.fuel.2023.130220>.

References

- Frenillot JP, Cabot G, Cazalens M, Renou B, Boukhalfa MA. Impact of H₂ addition on flame stability and pollutant emissions for an atmospheric kerosene/air swirled flame of laboratory scaled gas turbine. *Int J Hydrogen Energy* 2009;34(9):3930–44.
- Burguburu J, Cabot G, Renou B, Boukhalfa AM, Cazalens M. Effects of H₂ enrichment on flame stability and pollutant emissions for a kerosene/air swirled flame with an aeronautical fuel injector. *P Combust Inst* 2011;33(2):2927–35.
- Ma K, Peng W, Zheng J, Gu C, Zhang R, Liu Y, et al. Study on fracture strain of Cr-Mo steel in high pressure hydrogen. *Int J Hydrogen Energy* 2021;46(61):31501–9.
- Liu J, Ma H, Zheng S, Zhang Z, Zheng J, Zhao Y. Numerical investigation on temperature-rise of on-bus gaseous hydrogen storage cylinder with different thickness of liner and wrapping material. *Int J Hydrogen Energy* 2021;46(39):20607–20.
- Blazowski WS. Combustion considerations for future jet fuels. *Symp (Int) Combust* 1977;16(1):1631–9.
- Mohankumar S, Senthilkumar P. Particulate matter formation and its control methodologies for diesel engine: A comprehensive review. *Renew Sustain Energy Rev* 2017;80:1227–38.
- Johnson T, Joshi A. Review of vehicle engine efficiency and emissions. *SAE Int J Engines* 2018;11(6):1307–30.
- S. Webb PDW R.C Miake-Lye M.T. Timko T. G. Thrasher Airport Cooperative Research Program, Report 6, Transportation Research Board. Washington DC 2008.
- Sun Z, Dally B, Nathan G, Alwahabi Z. Effects of hydrogen and nitrogen on soot volume fraction, primary particle diameter and temperature in laminar ethylene/air diffusion flames. *Combust Flame* 2017;175:270–82.
- Gu M, Chu H, Liu F. Effects of simultaneous hydrogen enrichment and carbon dioxide dilution of fuel on soot formation in an axisymmetric coflow laminar ethylene/air diffusion flame. *Combust Flame* 2016;166:216–28.
- Akram MZ. Study of hydrogen impact on lean flammability limit and burning characteristics of a kerosene surrogate. *Energy* 2021;231:120925.
- Zeng W, Liu J, Liu Y, Chen B, Liu A. The effect of hydrogen addition on the combustion characteristics of RP-3 kerosene/air premixed flames. *Energies* 2017;10(8).
- Liu F, Ai Y, Kong W. Effect of hydrogen and helium addition to fuel on soot formation in an axisymmetric coflow laminar methane/air diffusion flame. *Int J Hydrogen Energy* 2014;39(8):3936–46.
- Khanehazar A, Cepeda F, Dworkin SB. The influence of nitrogen and hydrogen addition/dilution on soot formation in coflow ethylene/air diffusion flames. *Fuel* 2022;309:122244.
- Gülder ÖL, Snelling DR, Sawchuk RA. Influence of hydrogen addition to fuel on temperature field and soot formation in diffusion flames. *Symp (Int) Combust* 1996;26(2):2351–8.
- Akram MZ, Ma F, Akram MW. A numerical approach to elucidate the combustion and emission characteristics of n-dodecane under hydrogen enrichment. *Energy Convers Manage* 2022:255.
- Xu L, Yan F, Wang Y, Chung SH. Chemical effects of hydrogen addition on soot formation in counterflow diffusion flames: Dependence on fuel type and oxidizer composition. *Combust Flame* 2020;213:14–25.
- Honnet S, Seshadri K, Niemann U, Peters N. A surrogate fuel for kerosene. *P Combust Inst* 2009;32(1):485–92.
- Mensch A, Santoro RJ, Litzinger TA, Lee SY. Sooting characteristics of surrogates for jet fuels. *Combust Flame* 2010;157(6):1097–105.
- Dooley S, Won SH, Heyne J, Farouk TI, Ju Y, Dryer FL, et al. The experimental evaluation of a methodology for surrogate fuel formulation to emulate gas phase combustion kinetic phenomena. *Combust Flame* 2012;159(4):1444–66.
- Yu W, Yang W, Tay K, Zhao F. An optimization method for formulating model-based jet fuel surrogate by emulating physical, gas phase chemical properties and threshold sooting index (TSI) of real jet fuel under engine relevant conditions. *Combust Flame* 2018;193:192–217.
- He Y, Qi S, Liu S, Xin S, Zhu Y, Wang Z. Effects of the gas preheat temperature and nitrogen dilution on soot formation in co-flow methane, ethane, and propane diffusion flames. *Energy Fuel* 2021;35(9):7169–78.
- Qi S, Sun Z, Wang Z, Liu Y, He Y, Liu S, et al. Effects of gas preheat temperature on soot formation in co-flow methane and ethylene diffusion flames. *P Combust Inst* 2021;38(1):1225–32.
- Michelsen HA, Schulz C, Smallwood GJ, Will S. Laser-induced incandescence: Particulate diagnostics for combustion, atmospheric, and industrial applications. *Progress In Energy And Combustion Science* 2015;51:2–48.
- Liu F, Snelling DR, Thomson KA, Smallwood GJ. Sensitivity and relative error analyses of soot temperature and volume fraction determined by two-color LII. *Appl Phys B-Lasers O* 2009;96(4):623–36.
- Orain M, Baranger P, Ledier C, Apeloig J, Grisch F. Fluorescence spectroscopy of kerosene vapour at high temperatures and pressures: Potential for gas turbines measurements. *Appl Phys B* 2014;116(3):729–45.
- Mouis AG, Menon A, Katta V, Litzinger TA, Linevsky M, Santoro RJ, et al. Effects of m-xylene on aromatics and soot in laminar, N₂-diluted ethylene co-flow diffusion flames from 1 to 5atm. *Combust Flame* 2012;159(10):3168–78.
- Zhang Y, Xiao B, Li Y, Liu P, Zhan R, Huang Z, et al. LIF diagnostics for selective and quantitative measurement of PAHs in laminar premixed flames. *Combust Flame* 2020;222:5–17.
- Dasch CJ. One-dimensional tomography - A comparison of Abel, onion-peeling and filtered backprojection methods. *Appl Optics* 1992;31(8):1146–52.
- ANSYSChemkin 17.0 (15151). *Reaction Design, San Diego* 2015.
- Zhang T, Zhao L, Thomson MJ. Effects of n-propylbenzene addition to n-dodecane on soot formation and aggregate structure in a laminar coflow diffusion flame. *P Combust Inst* 2017;36(1):1339–47.
- Gao Z, Zhu L, Zou X, Liu C, Tian B, Huang Z. Soot reduction effects of dibutyl ether (DBE) addition to a biodiesel surrogate in laminar coflow diffusion flames. *P Combust Inst* 2019;37(1):1265–72.
- Gao Z, Cheng X, Ren F, Zhu L, Huang Z. Compositional effects on sooting tendencies of diesel surrogate fuels with four components. *Energy Fuel* 2020;34(7):8796–807.
- Ren F, Cheng X, Gao Z, Huang Z, Zhu L. Effects of NH₃ addition on polycyclic aromatic hydrocarbon and soot formation in C₂H₄ co-flow diffusion flames. *Combust Flame* 2022;241:111958.
- Saggese C, Frassoldati A, Cuoci A, Faravelli T, Ranzi E. A wide range kinetic modeling study of pyrolysis and oxidation of benzene. *Combust Flame* 2013;160(7):1168–90.
- Ahmed AM, Mancarella S, Desgroux P, Gasnot L, Pauwels JF, El Bakali A. Experimental and numerical study on rich methane/hydrogen/air laminar premixed flames at atmospheric pressure: Effect of hydrogen addition to fuel on soot gaseous precursors. *Int J Hydrogen Energy* 2016;41(16):6929–42.
- China National Standardization Technical Committee on Petroleum Products and Lubricants. NO.3 Jet fuel. GB/T 6537-2006[S]. Beijing Standards Press of China 2007:1-5. (in Chinese).
- Li A, Zhu L, Deng Z, Gao Z, Huang Z. A fundamental investigation into chemical effects of carbon dioxide on intermediate temperature oxidation of biodiesel surrogate with laminar flow reactor. *Energy* 2017;141:20–31.
- Schön A, Streibel T, Suntutz R, Bockhorn H. Numerical and experimental analysis of soot formation in laminar diffusion flames along selected particle tracks. *P Combust Inst* 2002;29(2):2399–405.
- Gülder ÖL, Snelling DR. Influence of nitrogen dilution and flame temperature on soot formation in diffusion flames. *Combust Flame* 1993;92(1):115–24.
- Wu J, Chen L, Bengtsson P-E, Zhou J, Zhang J, Wu X, et al. Effects of carbon dioxide addition to fuel on soot evolution in ethylene and propane diffusion flames. *Combust Flame* 2019;199:85–95.
- Snelling DR, Liu F, Smallwood GJ, Gülder ÖL. Determination of the soot absorption function and thermal accommodation coefficient using low-fluence LII in a laminar coflow ethylene diffusion flame. *Combust Flame* 2004;136(1):180–90.
- Santoro RJ, Yeh TT, Horvath JJ, Semerjian HG. The transport and growth of soot particles in laminar diffusion flames. *Combust Sci Technol* 1987;53(2-3):89–115.
- Johansson KO, Head-Gordon MP, Schrader PE, Wilson KR, Michelsen HA. Resonance-stabilized hydrocarbon-radical chain reactions may explain soot inception and growth. *Science* 2018;361(6406):997–1000.
- Kholghy MR, Kelesidis GA, Pratsinis SE. Reactive polycyclic aromatic hydrocarbon dimerization drives soot nucleation. *PCCP* 2018;20(16):10926–38.
- Frenklach M, Mebel AM. On the mechanism of soot nucleation. *PCCP* 2020;22(9):5314–31.
- Semenikhin AS, Savchenkova AS, Chechet IV, Matveev SG, Frenklach M, Mebel AM. On the mechanism of soot nucleation. II. E-bridge formation at the PAH bay. *PCCP* 2020;22(30):17196–204.
- Savchenkova AS, Semenikhin AS, Chechet IV, Matveev SG, Frenklach M, Morozov AN, et al. Mechanism of E-bridge formation by various PAH molecules: A theoretical study. *Chem Phys Lett* 2022;799:139637.